

Design and Experiments for Multi-Section-Transformable (MIST)-UAV

Ruben D'Sa and Nikolaos Papanikolopoulos

{dsaxx005}@umn.edu, {npapas}@cs.umn.edu

Department of Computer Science and Engineering, University of Minnesota

Abstract—Presented in this paper are the design and experiments for a transformable Vertical Take Off and Landing (VTOL) UAV. This work demonstrates shape-shifting transformation, building upon the conceptual designs put forth in [1] and [2], along with hardware prototyping and component testing from [3]. A deterministic model is presented to characterize the flight of the MIST-UAV in simulation. Experimental results from the platform demonstrate for the first time successful in-air transformation from multi-rotor, tail-sitter, and fixed-wing operation. Experiments also validated transformation repeatability, successfully testing multiple sequential transformations.

I. INTRODUCTION

The use of unmanned aerial vehicles (UAVs) has seen extensive development throughout industrial and academic domains. In recent years, many research groups have undertaken the task of designing highly maneuverable multi-rotor systems. Due to the use of vertical thrust as the primary source of lift, these multi-rotor systems are capable of operating in space constrained environments as shown in the work of [4], [5], and [6]. In multi-rotor flight, the dominant source of lift comes from the propulsion system while in fixed-wing flight, the dominant source of lift is produced by the aircraft's wings. For particular multi-rotor systems, the spatial maneuverability of multi-rotor flight can be augmented with the efficiency of fixed-wing flight. Multi-rotor and fixed-wing operation is achieved by utilizing flight state transformation. Recent work [7], [8], [9], demonstrates examples of transformation between flight states. One of the major challenges with these platforms is with regards to flight time. Even with the augmentation of multi-rotor and fixed-wing flight modes, these systems are limited by battery energy density. Research from [10], [11], and [12] demonstrate day-long and multi-day operation of fixed-wing solar powered flight. An energy surplus is made possible in fixed-wing flight by matching component efficiency at a system level and leveraging high aspect-ratio airframe design at low Reynolds numbers.

The work presented in this paper extends on the work from [1], [2], and [3] by demonstrating shape-shifting transformation in the Multi-Section-Transformable (MIST)-UAV platform. When applied to the SUAV-Q platform, it combines the efficiency of fixed-wing solar powered flight with the maneuverability of a compact multi-rotor airframe. The augmentation in energy is made possible through an airframe transformation shown in Figure 1. One of the goals in pursuing the development of the SUAV-Q platform is to serve as a tool for facilitating multi-application research. The



Fig. 1: MIST-UAV Prototype performing multi-rotor to fixed-wing transformation.

SUAV-Q platform enables operating under unique modalities as discussed in [13]. These modalities range from ground perching energy collection to alternating between high-level and low-level observations in fixed-wing and multi-rotor configurations. By alternating between these states, it is possible to utilize the energy surplus of solar-powered fixed-wing flight for the high energy expenditure of the multi-rotor flight state.

The goal of this paper is to demonstrate and evaluate the system characteristics of transformation on the MIST-UAV across multi-rotor, transformation, and fixed-wing states. Emphasis of analysis is placed on the transformation sequence needed to transition from multi-rotor to fixed-wing flight states. A discussion of aircraft geometry and design is made. Equations of motion are derived from first principles and used to guide simulations. The system architecture is detailed. Finally, results of experimental flights are presented and discussed. This is the first time that we were able to demonstrate these transformations in field experiments.

II. AERIAL ROBOT DESIGN

The MIST-UAV platform is a four-section transformable VTOL platform first introduced in [1]. While similar to the SUAV-Q, the MIST-UAV minimizes airframe weight by removing the solar power electronics and supporting hardware. The MIST-UAV platform is a highly actuated system, using a total of 11 actuators. Each wing section contains a propulsion motor and control-surface servo. Mounted between three of the four hinges are high torque servos used to initiate and facilitate transformation. Shown in Figure 2 is a CAD rendering of the MIST-UAV in three different hinge angle states. Hinge angles are continuous between 90° and 180° where the bounds correspond to multi-rotor and fixed-wing configurations respectively. Each wing section is designed to utilize an MH49 airfoil profile for its desirable aerodynamic characteristics as discussed in [3]. The design of each wing

section consists of a central mounted main spar that acts as the primary load-bearing component. Ribs are mounted along the length of the spar to form the airfoil profile. Forces and moments from the servo hinge during transformation are primarily distributed to the main spar to make for a weight efficient design.

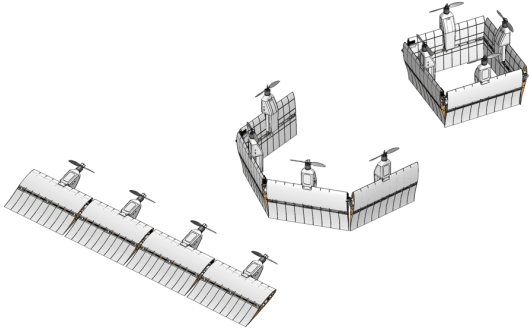


Fig. 2: MIST-UAV airframe with hinge angles of 180°, 120°, and 90°.

Some of the challenging aspects related to transformation are the changing inertial and aerodynamic characteristics of the system as the geometry of the airframe changes. Forward kinematics were used to compute the location of the link center of gravity as a function of hinge angle. Figure 3 shows the major actuators on each of the wing sections. Shown in Figure 4 is a diagram illustrating the forces and moments acting on a single wing section.

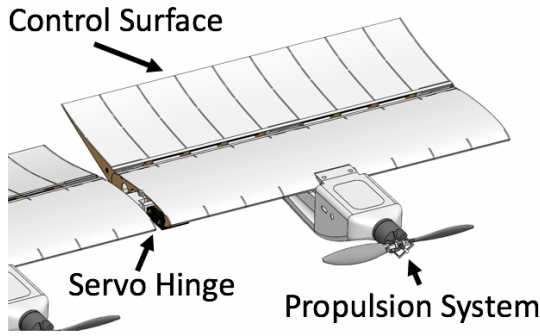


Fig. 3: Location of actuators on each wing section.

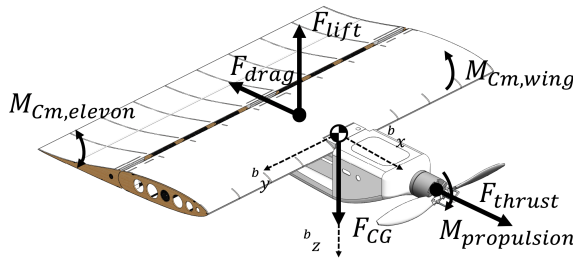


Fig. 4: Aerodynamic forces and moments acting on a single wing section.

III. EQUATIONS OF MOTION

Key parameters of a single wing section are listed in Table I. Aerodynamic polars related to lift C_L , drag C_D ,

pitching moment C_M , and control surface deflection $C_{\delta L}$ $C_{\delta D}$ $C_{\delta M}$ at varying Reynolds numbers and angle-of-attack were computed using XFLR5 [14]. Surfaces relating control surface deflection to lift, drag, and moment polars were computed to approximate the aerodynamic behavior of the system at various system states and flight conditions. Shown in Figure 7 and 8 is an example of how the coefficient of lift surface at high and low Reynolds number changes as a function of angle-of-attack, control surface deflections. These surfaces were computed for Re 5,000 to 400,000 at intervals of 5,000 and for pitching moment and drag coefficients.

Model Specifications	Value
Wingspan	2.15 m
Length	0.51 m
Chord Length	0.31 m
Height	0.09 m
$I_{wing,xx}$.198 kg m ²
$I_{wing,yy}$.146 kg m ²
$I_{wing,zz}$.148 kg m ²
Wing area (S)	0.634 m ²
Air density (ρ)	1.224 kg/m ²
Chord length (\bar{c})	0.312 m
Wing Span (b)	2.032 m
Total Mass	2300 g
X_{cm}	0.05 m

TABLE I: Key airframe specifications. Principle moments of inertia were computed from CAD models. X_{cm} is measured with respect to the quarter-chord line.

Below are the equations of motion used to describe the behavior of the transformer UAV. These equations were based on the aircraft dynamics from [15].

$$\begin{bmatrix} \{COG\}F \\ \{COG\}\tau \end{bmatrix} = \sum_{i=0}^3 \left[\begin{bmatrix} \{COG\}R_{\{i\}} * \{i\}F \\ \{COG\}R_{\{i\}} * \{i\}\tau - \{COG\}R_{\{i\}} * \{i\}F \end{bmatrix} \right] \quad (1)$$

where

$$\bar{q}S = \frac{1}{2}\rho v^2 S \quad (2)$$

$$\begin{aligned} \{i\}CX &= -CD\cos(\alpha) + CL\sin(\alpha) \\ \{i\}CZ &= -CD\sin(\alpha) - CL\cos(\alpha) \end{aligned} \quad (3)$$

$$\{i\}F = \begin{bmatrix} F_{Mi} + CX * \bar{q}S \\ CY * \bar{q}S \\ CZ * \bar{q}S \end{bmatrix} \quad (4)$$

and

$$\{i\}\tau = \begin{bmatrix} C_l\bar{q}SB \\ C_m\bar{q}S\bar{c} \\ C_n\bar{q}Sb \end{bmatrix} \quad (5)$$

Equation (1) represents the force and torque acting on the body-frame located at the overall system center-of-gravity (COG). This force and torque is the sum of the rotated forces and torques acting on each wing section. Looking at each individual wing section frame, body-axis coefficients are computed in Equation (3). The inertia tensor of the system in the body frame at COG was computed using a combination of forward kinematics and the parallel axis

theorem. The ordinary differential equations describing the rigid body motion of the system were numerically integrated using Runge-Kutta (4th order) to compute the system state consisting of translational and angular position and velocity. A simulation environment was built in Python to experiment with transformation trajectories as shown in Figure 6.

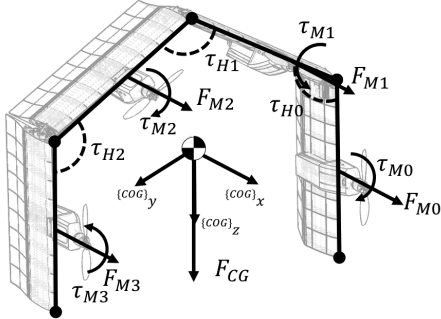


Fig. 5: Forces and moments induced by only the propulsion system and servo hinges in the COG frame.

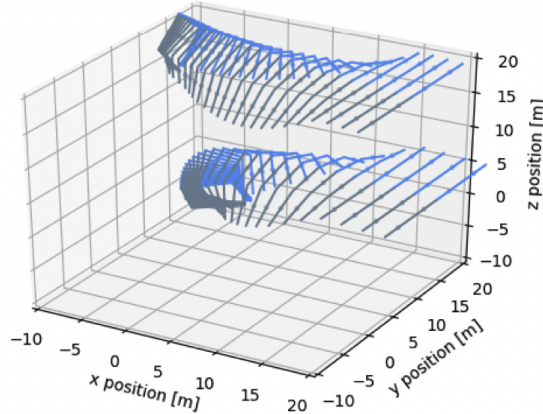


Fig. 6: Simulation of the MIST-UAV multi-rotor to fixed-wing transformation trajectory. Each dot along the line segment represents the wing section center of gravity. Two different simulations with different starting conditions are presented. The upper trajectory has a starting initial pose of pitch=0° while the lower trajectory is initialized at pitch=90°. An attitude controller is used to control the system with a roll, pitch, yaw setpoint = [0,0,0].

IV. PROTOTYPE SYSTEM ARCHITECTURE

The overall system architecture can be divided into three main sections; Sensors and Compute, Actuation, Transformation, and Power Distribution.

A. Sensors and Compute

The MIST-UAV consists of both on-board and off-board sensing and compute elements. On-board components consist of a HKPilot32 flight controller running a modified PX4 stack [16]. The HKPilot32 contains an internal IMU, magnetometer, and barometric pressure transducer. A separate radio telemetry system is used to communicate with a ground station running QGroundcontrol. A Raspberry Pi 3 Model B operates as a secondary compute module running as a Robot Operating System (ROS) node and communicates with the HKPilot32 over UART.

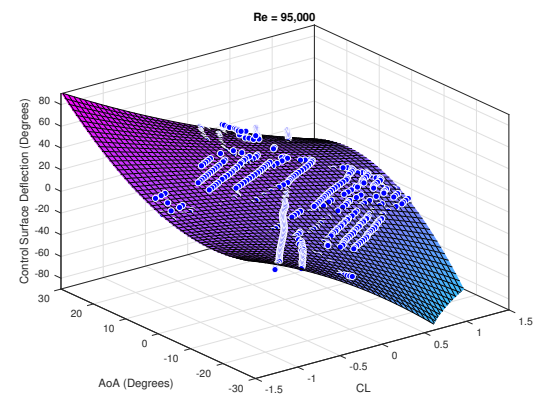


Fig. 7: CL as a function of control surface deflection and angle-of-attack (AoA) at $Re = 95,000$ for the MH49 airfoil.

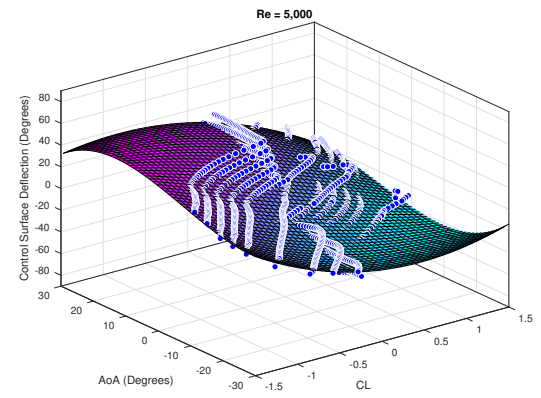


Fig. 8: CL as a function of control surface deflection and angle-of-attack (AoA) at $Re = 5,000$ for the MH49 airfoil.

The on-board ROS node is implemented using roscore and MAVROS. The node is controlled via an Ad-Hoc WiFi network by a ground station and is used to orchestrate the high level system functions. The high level commands are sent to the flight controller as desired position and attitude coordinates.

The flexibility of the Raspberry Pi allows it to easily communicate with other systems on board the UAV in order to inform the ROS node of the overall state of the system, such as battery state of charge, and any other states which are valuable to the mission being performed.

B. Actuation

Beyond the standard motors used for the propulsion system the MIST-UAV uses servo motors to power the transformation hinges and control surfaces. The distribution and specification of these motors and controllers can be seen in Figure 10.

C. Transformation

Transformation can be defined as any change in the geometrical shape or primary flight characteristics of the MIST-UAV. In cases related to multi-rotor hovering and fixed-wing translational flight, transformation is changing the system configuration from a multi-rotor configuration to

a fixed-wing configuration. Similarly in the case of fixed-wing translational flight and fixed-wing hovering flight (tail-sitter flight), transformation is the change in primary flight conditions. Transformation is performed in a three-stage process:

- 1) Exclusively run multi-rotor attitude and position controllers to track set-points published from either a ground control system or an off-board computing node on the aircraft.
- 2) Publish transformation specific setpoints to the multi-rotor position controller. Upon reaching a set of minimum conditions related to airspeed and attitude, the hinge actuators engage.
- 3) Upon reaching attitude thresholds, exclusively utilize fixed-wing attitude and position controllers for commanding actuators.

Shown in Figure 9 is an example of the roll component of the attitude controller used in a multi-rotor state. A similar architecture is used for yaw and pitch. The mixer block is responsible for distributing normalized commands [-1,1] to the PWM drivers, and ultimately all of the system actuators. A unique characteristic of the MIST-UAV is that the desired mapping from high-level commands (roll, pitch, yaw, altitude) to actuators changes depending on the system state. For instance, pitch while in a multi-rotor state is controlled by varying angular velocities of the motors. Alternatively, while in a tailsitter or fixed-wing state, pitch is controlled by control surface deflection. The mixer block is responsible for performing this mapping taking into account desired system state through the mode block.

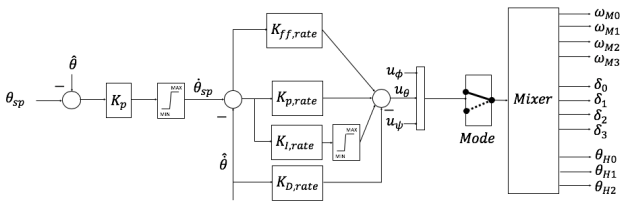


Fig. 9: Roll component of the multi-rotor attitude controller. $\hat{\theta}$ and $\hat{\dot{\theta}}$ are estimated using an Extended Kalman Filter. ω_{mi} is the angular velocity of the propulsion system, δ_i is the control surface deflection, and θ_i is the servo hinge angle.

D. Energy Management

Power is monitored at several points in the system using CSA (Current Sense Amplifiers). These devices, along with battery monitoring systems and data logging devices on board, are able to provide significant system information to the ROS network regarding available energy, which can be used to inform the flight plan. The energy management portion of the system also consists of power converters, which are necessary to provide stable logic level 5V power, along with a high current 7V power supply for the servo motors (which can be seen in Figure 10).

E. Distributed Battery System

The propulsion system on the MIST-UAV is the primary source of energy expenditure. Given that high current power

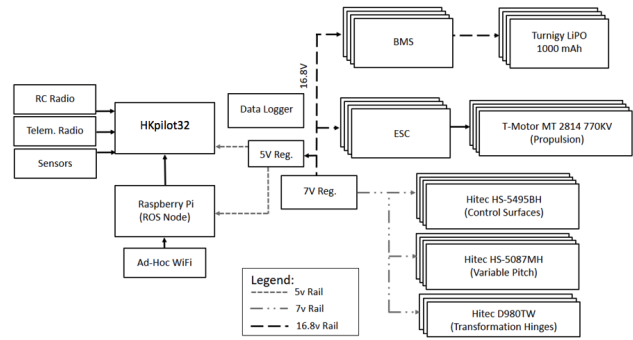


Fig. 10: High-level layout of the electrical components of the aircraft, showing the distribution of the various power rails, along with the various communication systems on board.

rails must be routed through the airframe, managing parasitic losses in the power distribution system is of high importance. This is particularly important with regards to voltage between the high current rail and the propulsion system. Significant voltage drop can result in failure to reach desired propeller angular velocity. Shown in Figure 11 is an example of two different battery configurations. By distributing a given battery capacity across multiple batteries along the perimeter of the frame, voltage drop between the propulsion system and voltage source can be minimized. Shown in Table II is a list of electronics and their corresponding system mass. These components are distributed throughout the wing sections to provide a close to centrally spaced center-of-gravity in a multi-rotor state.

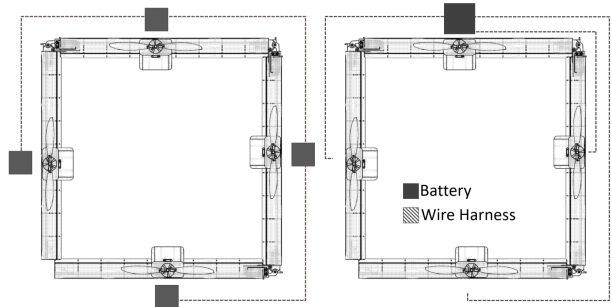


Fig. 11: Graphical representation of two wire harness layout structures, bus topology (left) and star pattern (right).

Electronics	Unit Mass [g]
Battery (1Ah)	170
Telem. Radio	60
MPPT	45
RPI	45
7v Reg	40
HkPilot32	38
GPS	35
ESC	30
Data Logger	28
WiFi Ant.	25
Pitot Tube	20
5v Reg	10
RC Receiver	4

TABLE II: Masses of the various electrical components utilized on the airframe. These masses are used to determine the appropriate pods in which the items should be placed in order to most evenly distribute the electrical system mass.



Fig. 12: MIST-UAV prototype performing multi-rotor to fixed-wing to multi-rotor transformation.

V. EXPERIMENTAL RESULTS

Utilizing the design and system architecture discussed in Sections II and IV, a MIST-UAV prototype was fabricated and several successful transformation test flights were performed.

A. Prototype

Shown in Figure 13 is the MIST-UAV prototype pictured during mid transformation. The airframe used a carbon-fiber main spar interleaved with laser cut basswood ribs. The skeleton frame was then wrapped in Monokote to form an aerodynamic surface. This particular MIST-UAV prototype was configured with fixed-pitch propellers to simplify prototype complexity. Two 4-cell 1Ah Li-po batteries were used and mounted in opposing wing sections for weight distribution, but electrically connected to same high current rail.

B. Transformation and Flight Performance

Shown in Figure 12 is a side view of the MIST-UAV prototype performing transformation. The system takes-off in a multi-rotor state, transforms into a fixed-wing state, and transforms back into a multi-rotor state to land. Shown in Figure 14 are plots showing the power and vehicle characteristics during this flight. Only the attitude controllers were enabled throughout this test flight. Angular positions

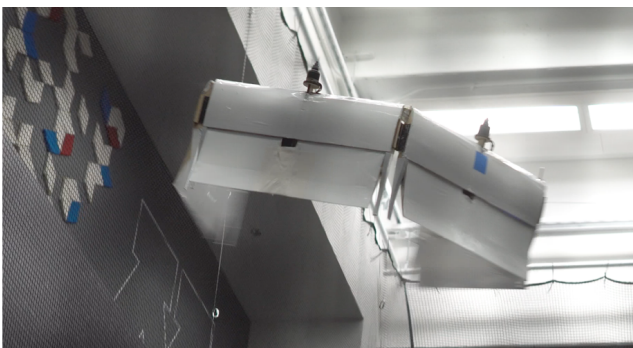


Fig. 13: MIST-UAV prototype in between multi-rotor and fixed-wing transformation.

in both multi-rotor and fixed-wing states were manually commanded. Full transformation was commanded using the Aux signal as shown in Figure 14. While operating in a multi-rotor state, only the propulsion system was used to control attitude. This was done to prevent the control surfaces from internally crashing with one another and decreasing the effective thrust of the propulsion system.

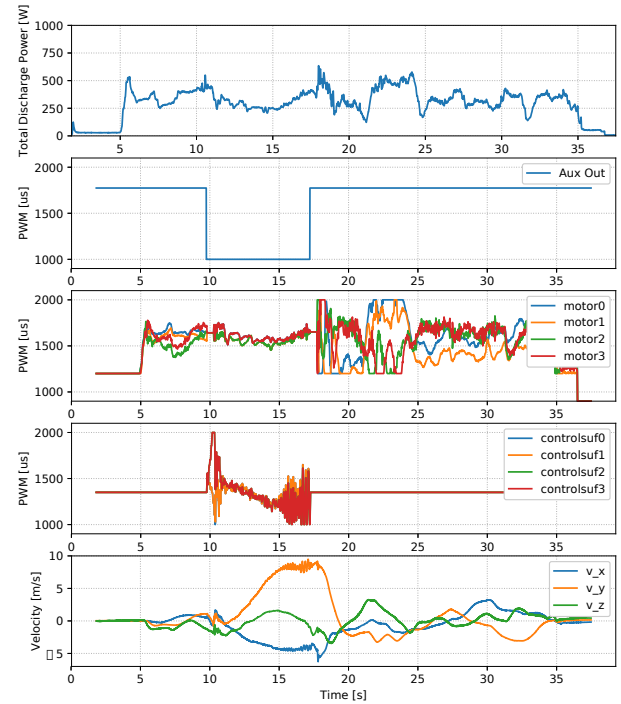


Fig. 14: Flight characteristics during multi-rotor to fixed-wing to multi-rotor transformation.

During initial multi-rotor flight, average power consumption was 347.8W. After transformation while in a fixed-wing state, average power consumption dropped to 297.9W. Transforming back into multi-rotor state, average power consumption was 346.1W. Peak power consumption occurred at transformation initiation points, 556.2W and 638.03W re-

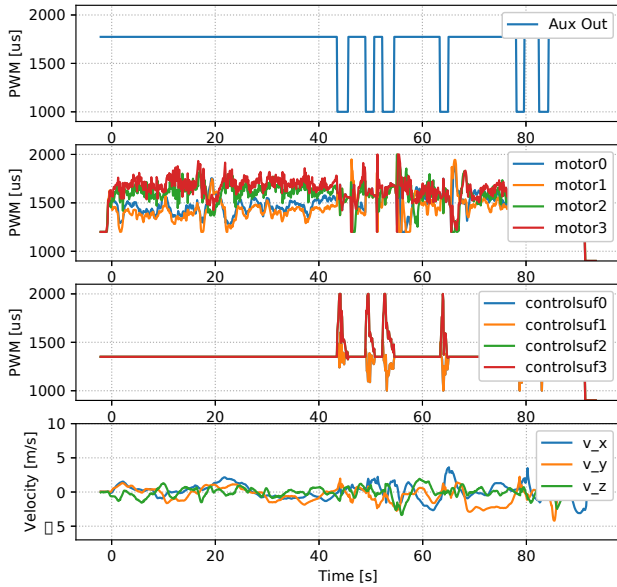


Fig. 15: Flight characteristics during six times multi-rotor tailsitter multi-rotor transformation.

spectively. On average, full open to full close transformations were performed in 0.5s. Due to fabrication techniques, and the lack of a full trailing edge MH49 profile, power consumption during fixed-wing flight was higher than expected as the airframe was likely not generating as much lift as possible with an accurate MH49 profile. Figure 15 demonstrates the repeatability of transformation, transforming from multi-rotor to tailsitter and back six times in a single flight.

VI. CONCLUSION

Presented in this paper are the design and experiments of a multi-section transformable UAV. This work builds upon the work from [2] and [3], focusing primarily on demonstrating successful shape-shifting transformation. The aerial robot design of the MIST-UAV is presented describing key and unique features of the platform. The equations of motion are presented utilizing XFLR5 to approximate the aerodynamic polars across the system operating range. The prototype system architecture is presented describing the interconnection between several electronic and algorithmic components used for transformation. A distributed battery system is presented to supply current to high power components such as the propulsion system with minimal losses and wire harness mass. Finally, a prototype of the MIST-UAV is presented along with successful multi-rotor to fixed-wing to multi-rotor transformation. Power consumption during the flight was monitored along with commanded propulsion system and system velocities. Average power consumption during fixed-wing flight was found to be roughly 48.2W less than multi-rotor flight. However, average power consumption is likely to be significantly less during a fixed-wing flight with a more accurate wing section profile. Repeatability of transformation is validated by performing six sequential transformations with high frequency.

VII. ACKNOWLEDGEMENTS

This material is based upon work partially supported by the National Science Foundation through grants IIS-1427014, CNS-1439728, CNS-1531330, and CNS-1544887. Sentera Inc. and Honeywell Inc. have also supported parts of this work. Ruben D'Sa was supported by a National Science Foundation Graduate Research Fellowship No. 00039202.

REFERENCES

- [1] R. D'Sa, D. Jenson, and N. Papanikopoulos, "SUAV:Q - A Hybrid Approach To Solar-Powered Flight," *IEEE International Conference on Robotics and Automation (ICRA)*, pp. 3288–3294, May 2016.
- [2] R. D'Sa, D. Jenson, T. Henderson, J. Kilian, B. Schulz, M. Calvert, T. Heller, and N. Papanikopoulos, "SUAV:Q - An Improved Design for a Transformable Solar-Powered UAV," *IEEE/RSJ International Conference on Intelligent Robots and Systems (IROS)*, October 2016.
- [3] R. D'Sa, T. Henderson, D. Jenson, M. Calvert, T. Heller, B. Schulz, J. Kilian, and N. Papanikopoulos, "Design and Experiments for a Transformable Solar-UAV," *IEEE International Conference on Robotics and Automation (ICRA)*, May 2017.
- [4] D. W. Yoo, H. D. Oh, D. Y. Won, and M. J. Tahk, "Dynamic modeling and control system design for tri-rotor uav," in *2010 3rd International Symposium on Systems and Control in Aeronautics and Astronautics*, June 2010, pp. 762–767.
- [5] Y. Long and D. J. Cappelleri, "Complete dynamic modeling, control and optimization for an over-actuated mav," in *2013 IEEE/RSJ International Conference on Intelligent Robots and Systems*, Nov 2013, pp. 1380–1385.
- [6] M. Zhao, T. Anzai, F. Shi, X. Chen, K. Okada, and M. Inaba, "Design, modeling, and control of an aerial robot dragon: A dual-rotor-embedded multilink robot with the ability of multi-degree-of-freedom aerial transformation," *IEEE Robotics and Automation Letters*, vol. 3, no. 2, pp. 1176–1183, April 2018.
- [7] J. E. Low, L. T. S. Win, D. S. B. Shaiful, C. H. Tan, G. S. Soh, and S. Foong, "Design and dynamic analysis of a transformable hovering rotorcraft (thor)," in *2017 IEEE International Conference on Robotics and Automation (ICRA)*, May 2017, pp. 6389–6396.
- [8] S. Verling, B. Weibel, M. Boosfeld, K. Alexis, M. Burri, and R. Siegwart, "Full Attitude Control of a VTOL Tailsitter UAV," in *2016 IEEE International Conference on Robotics and Automation (ICRA)*, May 2016, pp. 3006–3012.
- [9] S. Verling, T. Stastny, G. Bttig, K. Alexis, and R. Siegwart, "Model-based transition optimization for a vtol tailsitter," in *2017 IEEE International Conference on Robotics and Automation (ICRA)*, May 2017, pp. 3939–3944.
- [10] S. Morton, L. Scharber, and N. Papanikopoulos, "Solar powered unmanned aerial vehicle for continuous flight: Conceptual overview and optimization," in *IEEE International Conference on Robotics and Automation (ICRA)*, 2013, pp. 766–771.
- [11] A. Noth, R. Siegwart, and W. Engel, "Autonomous solar UAV for sustainable flights," in *Advances in Unmanned Aerial Vehicles*, ser. Intelligent Systems, Control and Automation: Science and Engineering. Springer Netherlands, 2007, vol. 33, pp. 377–405.
- [12] P. Oettershagen, A. Melzer, T. Mantel, K. Rudin, R. Lotz, D. Siebenmann, S. Leutenegger, K. Alexis, and R. Siegwart, "A Solar-Powered Hand-Launchable UAV for Low-Altitude Multi-Day Continuous Flight," in *IEEE International Conference on Robotics and Automation (ICRA)*, May 2015, pp. 3986–3993.
- [13] D. Jenson, R. D'Sa, T. Henderson, J. Kilian, B. Schulz, and N. Papanikopoulos, "Energy Characterization of a Transformable Solar Powered UAV," *IEEE/RSJ International Conference on Intelligent Robots and Systems (IROS)*, October 2017.
- [14] A. Deperrois, "Stability Analysis Using XFLR5," http://www.xflr5.com/docs/XFLR5_and_Stability_analysis.pdf, 2010.
- [15] R. F. Stengel, *Flight dynamics*. Princeton University Press, 2015.
- [16] "PX4 Dev Guide," <http://dev.px4.io/>, 2016.